AIAA 93-3536

Three Dimensional Aerodynamic Analysis of a High-Lift Transport Configuration

Simha S. Dodbele
ViGYAN, Inc.
Hampton, Va

AIAA Applied Aerodynamics Conference
August 9-11, 1993 / Monterey, CA

THREE DIMENSIONAL AERODYNAMIC ANALYSIS OF A HIGH LIFT TRANSPORT CONFIGURATION

Simha S. Dodbele*
ViGYAN Inc.
30 Research Dr.
Hampton, VA 23666

Abstract

Two computational methods, a surface panel method and an Euler method employing unstructured grid methodology, were used to analyze a subsonic transport aircraft in cruise and high-lift conditions. The computational results were compared with two separate sets of flight data obtained for the cruise and high-lift configurations. For the cruise configuration, the surface pressures obtained by the panel method and the Euler method agreed fairly well with results from flight test. However, for the high-lift configuration considerable differences were observed when the computational surface pressures were compared with the results from high-lift flight test.

On the lower surface of all the elements with the exception of the slat, both the panel and Euler methods predicted pressures which were in good agreement with flight data. On the upper surface of all the elements the panel method predicted slightly higher suction compared to the Euler method. On the upper surface of the slat, pressure coefficients obtained by both the Euler and panel methods did not agree with the results of the flight tests. A sensitivity study of the upward deflection of the slat from the 40° flap setting suggested that the differences in the slat deflection between the computational model and the flight configuration could be one of the sources of this discrepancy.

The computation time for the implicit version of the Euler code was about 1/3 the time taken by the explicit version though the implicit code required 4 times the memory taken by the explicit version.

Nomenclature

C	Reference wing chord at 2Y/b=0.6, ft.
C_p	Pressure coefficient, $(p-p_\infty)/qS_{ref}$
C_D	Drag coefficient, $Drag/qS_{ref}$
C_L	Lift coefficient, $Lift/qS_{ref}$
C_m	Pitching moment coefficient, Pitching moment/cqS_{ref}
C_f	Skin friction coefficient
L	Length of the fuselage, 89.54 ft.
M	Freestream Mach number
p	Local static pressure, $lbs/ft.^2$
p_∞	Free stream static pressure, $lbs/ft.^2$
q	Dynamic pressure, $lbs/ft.^2$
b/2	Semispan, 45 ft.
S_{ref}	Reference area, 980 $ft.^2$
X, Y, Z	Dimensional Cartesian coordinate system with the nose of the airplane at X=130",Y=0, Z=0
α	Aircraft angle of attack, deg.
ϕ	Circumferential angle, (ϕ=0 on the upper centerline) $\tan^{-1}$ [Y/(Z-227.05)], deg

Abbreviations

TSRV	Transport Systems Research Vehicle
2-D	Two-dimensional
3-D	three-dimensional

Introduction

The subject of high-lift systems has always been an area of special interest to aircraft designers. Accurate prediction of surface-pressure distributions, confluent boundary-layers, viscous wakes, separated flow in the cove region, and separated flow regions over multi-element high-lift wings play an essential role in the design of advanced high-lift systems[1]. The flow field around a multi-element high-lift wing is very complex and highly interactive. As part of a subsonic-transport high-lift research program, a multi-phased flight program is underway using the NASA-Langley Transport Systems Research Vehicle (TSRV) aircraft to obtain detailed full-scale flow measurements of the 5-element high-lift system at various flight conditions[2, 3]. The availability of detailed measurements of pressure distributions and boundary layer flow parameters is critical to the validation and development of computational methods. The complexities in the multi-element flow field have so far restricted most of the computational research investigations to two-dimensional flow (2-D) and quasi-three-dimensional flow investigations[2-9]. This research paper mainly focuses on modelling the complex three-dimensional

*. Research Scientist, Associate Fellow AIAA

flow field of the multi-element high-lift TSRV configuration (Boeing 737-100). Using three-dimensional (3-D) methods, it is beneficial to identify regions of predominantly 2-D flow, highly interactive regions involving three dimensional flow and vortex dominated regions. These studies can then be used to direct the appropriate computational methods for analyzing the flow physics around the complicated multi-element high lift system. Though the multi-element high-lift systems involve several regions of viscous flow, some of the dominant inviscid flow features can be studied through a 3-D inviscid analysis. These features include aspects such as strong wake vortex roll-up from the spanwise tips of the high-lift systems, which are frequently more powerful than the tip vortices associated with cruise wings, significant spanwise compressibility effects, etc.

In this paper, two methods have been used for computational analyses: a surface panel method based on potential flow and an Euler method based on unstructured grid methodology. Before attempting an analysis of the complex high-lift configuration, the simpler cruise configuration was analyzed. This was done in order to assess the performance of the two analysis methods without introducing the complexities associated with the high-lift system. The two methods were then applied to study the high-lift configuration. The results obtained from the computational analyses of the cruise configuration are compared with data obtained on the fuselage in a flight test[10] conducted under a viscous drag reduction program at NASA Langley Research Center. The computational results from the analysis of the high-lift configuration are compared with data obtained in a different flight test[3] conducted under a high-lift program also at NASA Langley Research Center. In the computational study involving the cruise configuration, the fuselage, horizontal and vertical tail assembly and cruise wing were modelled. In the high-lift study, the fuselage, horizontal and vertical tail assembly, inboard-wing, mid-wing, outboard-wing, leading edge slats and triple slotted flap system were modelled. The triple slotted flap system for the inboard-wing was not modelled in the high-lift study. Additionally, the engine and pylons were not modelled in either study.

Computational Analyses

The three-dimensional surface panel method VSAERO[11] was used as one of the computational methods for analyzing the cruise and high-lift configurations. The program VSAERO uses piecewise constant source and doublet singularities on quadrilateral panels representing the surface of the configuration. Source strengths are solved directly from the external Neumann boundary condition using the normal component of the external flow. A set of linear equations are obtained with doublet strengths as the unknowns by imposing the internal Dirichlet boundary condition of zero perturbation potential inside the configuration. The set of linear equations are solved either by a direct method or by a blocked Gauss-Siedel iterative procedure depending upon the number of unknowns in the equations. The gradient of the doublet potential distribution is used to obtain the surface perturbation velocities. The wakes downstream of the trailing edges of the multi-element system are modelled as thin wake panels. The wake shapes change at the end of each wake iteration in order to satisfy the force-free conditions on the wake panels. A converged wake shape is obtained when the wake shapes cease to change with the wake iterations after which surface pressure distributions are obtained. The overall aerodynamic forces can be obtained by integrating the surface pressure distributions.

An Euler method using unstructured grid methodology was used as the other computational method. An efficient Euler equation solver, USM3D[12], was used to obtain the flow solutions on the unstructured tetrahedral grid system around the cruise and the high-lift configurations. This solver is based on an upwind, cell centered, finite volume method. Explicit as well as the implicit versions[13,14] of USM3D code were used to obtain computational results. The explicit version uses the 3-stage Runge-Kutta time stepping scheme with local time stepping and implicit residual smoothing. The implicit scheme uses the linearized, backward Euler time differencing approach to update the solution at each time step. Details of the implicit algorithm are described in Ref. 14. The unstructured grids were generated by using a modified version of the program VGRID3D[15] which is an interactive tetrahedral grid generator based on the advancing-front concept[15]. Utilizing a new 'structured background grid' concept[16], a smooth grid size variation is achieved by solving an elliptic partial differential equation on the uniform Cartesian background grid. The desired distribution of grid spacing parameters in the field is obtained by specifying a number of 'point' and 'line' sources, and solving a Poisson equation on the Cartesian grid. Over the past few years, VGRID3D and USM3D have been successfully applied to several complex 3-D configurations[15,16,17]. This is the first time VGRID3D has been applied to develop unstructured grids on a 3-D high-lift aircraft configuration and also, this is the first time Euler calculations have been made on a 5-element high-lift aircraft configuration in subsonic flow using unstructured grids.

Computational Results

(a) The Cruise Configuration

The TSRV cruise configuration is a relatively easy configuration to model computationally compared to the more complex high-lift configuration. The cruise configuration was analyzed using the surface panel method, VSAERO and the explicit Euler method, USM3D. For the VSAERO calculations, a total of 2215 quadrilateral panels were generated to represent the cruise configuration. Wakes from the trailing edges of the cruise wing, horizontal tail, vertical tail and the back end of the fuselage were modelled. The first wake line from the cruise wing was fixed to the side of the fuselage and held rigid during the wake iterations. The rest of the wake lines were allowed to move freely. A jet type wake was prescribed for the wake trailing from the back end of the fuselage. Surface panels generated on the right side of the cruise configuration are presented in Fig. 1. The wakes trailing from different components of the configuration are also seen in the figure. For the Euler calculations, the unstructured grid was generated using VGRID3D. Figure 2 illustrates the unstructured surface grid on the cruise configuration. The entire computational grid consisted of 685000 tetrahedrons and a total of 124473 nodes representing one half of the complete configuration. A total of 30090 boundary surfaces and 15047 boundary nodes were used to model the configuration surface, outer boundaries and plane of symmetry.

The results obtained by the two computational methods on the cruise configuration were compared with the flight test results[10]. In the flight test, static pressures were measured at several longitudinal stations along the fuselage centerline and also in the circumferential direction on the fuselage at several longitudinal sections. Figure 3 presents comparisons of pressure coefficients obtained using VSAERO and USM3D, on the top symmetry line of the fuselage. These results correspond to $M = 0.5$ and $\alpha = 6.87^{\circ}$. Pressure coefficients obtained from surface pressure measurements from the flight experiment between the longitudinal station X/L=0.402 and X/L=0.763 (the beginning of the vertical tail surface) are also shown for comparison. The panel method predicts higher suction pressures compared to the Euler method at locations downstream of the windshield up to about 25% of the fuselage length from the nose. In the mid-section where the fuselage is flatter in the longitudinal direction the panel method and the Euler method predict pressures which are in very good agreement with the pressures measured in the flight test. Figure 4 presents the chordwise pressure distributions computed by VSAERO and USM3D at a spanwise wing section of $2Y/b = 0.6$. Since the main aim of the flight tests[10] was to conduct flow investigation on the fuselage, pressures were measured only on the fuselage and not on the cruise wing. As seen in the figure, on the upper surface near the leading edge, the panel method again predicts higher suction pressures compared to the Euler method. However, the results from the panel method and the Euler method are in good agreement for most of the wing section. Figure 5 presents pressure distributions obtained using the two computational methods in the circumferential direction on the top of the fuselage at the longitudinal station X/L=0.402. The experimental results are also presented for comparison. As seen in Fig.5, results from both the computational methods are close to the pressures from the flight experiment, although VSAERO tends to overpredict the suction levels slightly.

From the above discussion we can infer that for this simple cruise configuration, surface pressures can be predicted reasonably well by any of the two computational methods, the panel method or the Euler method. The performance of these two computational methods when applied to a complex high-lift configuration is discussed in the next section.

(b) The High-Lift Configuration

The more complex, high-lift configuration was analyzed using the two computational methods with a fixed flap setting of 40°. At this flap setting, the aircraft is in a landing mode with the inboard slat in a partially extended position and the two outboard slats in the fully extended position. The two outboard slats were modelled as a single slat since both the slats are set at fully extended position and at the same orientation to the wing. The inboard high-lift system was not modelled in the study.

The surface panel distribution generated on the starboard side of the high-lift configuration by VSAERO is presented in Fig. 6. A total of 3787 surface panels were generated and distributed in 36 patches on the configuration. Panels were densely distributed on the high-lift components and sparsely distributed on the fuselage and tail (see Fig. 6a). Wakes were modelled from the trailing edges of the three leading edge slats, wing and triple slotted flap system. Again, the first wake line from the inboard wing was fixed to the side of the fuselage and held rigid during the wake iterations. The rest of the wake lines were allowed to move freely. The panel method solutions presented here are after 6 wake iterations. A close-up view of the surface panels on the triple-slotted flap system is shown in Fig. 6b.

For the Euler calculations, a total of 743,304 tetrahedrons were generated in the flow field with 28,073 triangular faces representing the surface of the configuration. The unstructured surface grid on the configuration is presented in Fig. 7. The surface grid was deliberately made sparse on the fuselage and dense on the high-lift wing to get a better resolution grid on the high-lift elements (see Fig. 7a). The grid is stretched in the spanwise direction to keep the total number of tetrahedrons reasonable and at the same time getting a good distribution of grid points in the chordwise direction. Detailed view of the unstructured surface grid on the triple-slotted flap system is shown in Fig. 7b. Additional care was taken to concentrate cells near the leading and trailing edges of the high-lift elements. This was accomplished by carefully choosing proper magnitude and directions for the point and line sources in VGRID3D[14].

During the flight test under the high-lift program, static pressures were measured on the upper and lower surfaces of the slat, wing and triple slotted flap system at two different spanwise stations, one on the inboard section and the other in the midsection, at the spanwise station approximately 2Y/b=0.6 (Y=323"). The pressures measured at 2Y/b=0.6 are used in this paper to assess the computational results. A sectional view of the multi-element wing at 2Y/b=0.6 is shown in Fig. 8. Two angles of attack, α= 6.250° and 7.617°, were chosen for this computational study. These angles of attack are close to aircraft approach angle during landing. In the next section computational analysis for these angles of attack are discussed.

(1) High-lift Configuration at α =6.250°

Computational results obtained for the high-lift configuration at α = 6.250°, M = 0.2420 and at the flap setting of 40° are presented in Figs. 9a-9e. In the figures the pressure distributions obtained by both the computational methods are compared with the flight data at the spanwise section 2Y/b=0.6. The implicit version of the code USM3D was used to obtain Euler results. On the upper surface of the slat, both the panel and the Euler methods predict lower suction compared to the flight results (Fig.9a).

For the wing, as shown in Fig. 9b, both the methods predict lower suction compared to the flight test results with the panel method predicting slightly larger suction than the Euler results. Both the computational methods fail to predict the suction peak near the leading edge. On the lower surface, the surface pressures from the Euler calculations as well as the panel method are in excellent agreement with flight data except near the trailing edge where predictions from the Euler method are much better.

The surface pressures on the foreflap, midflap and aftflap from the two computational methods are compared with the results of the flight experiment in Figs. 9c-9e. For up to 50% of the foreflap, the Euler method predicts slightly lower flow acceleration on the upper surface. The panel method on the other hand predicts flow acceleration very well on the upper surface of the foreflap. Towards the trailing edge of the foreflap upper surface, the experimental pressure coefficients level off departing from the predictions from both the computational methods. It is reported in Ref. 2 that for this flap setting and all $\alpha \geq -0.5$, flow separated near the upper surface trailing edge of the foreflap as evidenced by near-zero C_f and this separation could have been the result of the complex boundary layer flow development over the slat and the main wing and its effect on the foreflap. On the lower surface, results from the Euler calculations are in much closer agreement with the flight test results than the results from the panel method.

For the midflap, as seen in Fig. 9d, the surface pressures obtained from the panel method and the Euler method are slightly higher than the flight test results on the entire lower surface. On the upper surface, the suction predicted from the panel method is higher than the flight results on the entire upper surface. The Euler andd paneel method calculations predict higher suction near the leading edge of the midflap.

Figure 9e presents the pressure distributions on the aftflap. On the upper surface, the suction obtained by the panel method are much higher than the experimental results. The pressures from Euler calculations are in excellent agreement with the flight test results in spite of the strong boundary layer flow coming from the forward lifting surfaces. On the lower surface of the aftflap, both the panel and the Euler calculations predict slightly higher pressures than the flight pressures.

(5) High-lift configuration at α = 7.617°

Computational results were obtained for the conditions α=7.617° and M= 0.1722 and are presented in Fig. 10. Two sets of flight data are used here for comparisons. Flight data used for the slat and wing correspond to the conditions α=7.700° and M= 0.1956 and flight data used for the triple slotted system correspond to the conditions α=7.617° and M= 0.1722. It is believed that this small change in the flight conditions on the slat, wing and the triple slotted flap system does not change the general conclusions drawn in this paper. In Fig. 10 results obtained from the panel method and the results from both the explicit as well as implicit Euler calculations are presented. As it is seen in

Fig. 10 there is not much difference between the pressure coefficients obtained from the two types of Euler calculations.

As seen in Fig. 10a, on the upper and lower surfaces of the slat, pressure coefficients obtained by both the Euler and panel methods do not agree with the results of the flight tests (Fig. 10a). On the wing, the computational methods underpredict suction on the entire upper surface and both the methods fail to capture the suction peak near the leading edge observed in the flight test (Fig. 10b). On the lower surface of the wing, except near the trailing edge, there is an excellent agreement of pressures predicted by the computational methods with the flight data. The results from the Euler calculations are much better than the panel method results near the trailing edge.

Comparison of the surface pressures on the foreflap from the computational methods along with the results from the flight experiment are presented in Fig. 10c. On the upper surface of the foreflap, the results from the panel method are closer to the flight test results and the Euler calculations predict lower flow acceleration. But on the lower surface the results from Euler calculations are in good agreement with the flight data. On the midflap, as seen in Fig. 10d, the surface pressures obtained from the Euler methods are in slightly better agreement with the results of the flight experiment than the panel method results. The panel method overpredicts the suction on the upper surface. The Euler methods also predicts higher suction on the first 50% of the upper surface.

As seen in Fig. 10e, on the upper surface of the aftflap, the results from the Euler calculations agree very well with the flight test results. On the upper surface, the panel method predicts higher suction than the experimental results and on the lower surface, the panel method predict slightly higher pressures than the flight pressures.

From these two angle of attack studies it is apparent that the Euler method predicted pressures on the aftflap which are in excellent agreement with the flight test results in spite of strong boundary layer flow coming from the forward elements. On part of the upper surfaces of the foreflap Euler calculations predicted lower suction than the flight test results. On the lower surface of the elements with the exception of the slat, both the panel and Euler methods predict pressures which are in good agreement with flight data. On the upper surface of the wing both the computational methods underpredict suction.

Generally, on the upper surface of all the elements the panel method predicted slightly higher suction compared to the Euler method. On the upper surface of the slat, pressure coefficients obtained by both the Euler and panel methods do not agree with the results of the flight tests. In order to understand this discrepancy, sensitivity of the slat deflection on the pressures were studied using the panel method. Figure 11 presents changes in the pressure distribution on the slat due to 5° and 10° upward slat deflections from the 40° flap setting position for $\alpha=6.250^{\circ}$. From the figure it is seen that 10° upward deflection of the slat brings the computational pressures closer to the pressures measured in the flight experiments. This suggested that the discrepancy in the slat pressures between the computations and the flight experiment shown in Figs. 9a and 10a are possibly caused by differences in slat deflections in the computational model and in the actual aircraft. Another possible reason for this desrepancy could be the effect of aeroelastic deflections in flight.

Flow Field Characteristics

It is of considerable interest to visualize the wakes trailing from the slats and the flaps to understand the flow physics of the high-lift configurations. Fig. 12 shows Mach number contours around the 5-element configuration at $\alpha=7.617^{\circ}$ and at the spanwise station of $2Y/b=0.6$. In the same figure the wakes from surface panel method are also presented. In Fig. 13 the total pressure contours calculated by the implicit Euler method at $\alpha=7.617^{\circ}$ and at $X/L=0.828$ are presented. The wake from the inboard and outboard spanwise tips of the triple slotted flap system can be clearly seen from the Euler computations. It is also clear from the figure that the vortex structure from the outboard spanwise tip of the triple slotted flap system is stronger than the vortex structure from the inboard spanwise tip of the flap system. The vortex from the spanwise tip of the wing is also seen in the figure and is just beginning to form.

Panel Method-computational Issues

In the high lift-configuration, one has to deal with several highly complex wake shapes trailing from the various elements of the high-lift components. As seen in the previous discussions on high-lift configuration, the panel method, VSAERO predicted higher suction on the upper surfaces than the Euler methods. Some of these differences could be traced to the wake treatments in the panel method. When the wake from the slat was initially fixed at a small distance above the wing, they had a tendency to bend inboard and pass very close to the control points on the panels of the downstream lifting surfaces. This would cause the solution to diverge after 3 to 4 iterations. In order to avoid divergence in the solutions, the initial wakes from the slat was allowed to

trail downstream at a steep angle up to a distance of about 1/5 wing chord lengths in the longitudinal direction and about 1/5 wing chord lengths in the direction normal to the wing and then allowed to trail at a constant height of 1/5 chord lengths above the wing. This procedure would keep the solutions stable during the wake iterations and also leads to a converged wake. However, it was found that slightly different wake shapes as starting solutions would converge to totally different "non-unique" wake.

In the calculations, it was also found desirable to put panels with large mutual influence in the same block during matrix inversion. However, the limitation on the block size in the Gauss-Siedel solution procedure put a restriction on the number of panels allowed in the streamwise direction. This limitation restricted the number of panels allowed in the streamwise direction. This limitation in the block size was found to be very critical for multi-element part-span high-lift configurations.

It was also found that the "Global" wake-grid-planes option present in the panel method restricted the total number of wake panels and hence the size of the panels immediately aft of the trailing edges of the lifting elements. This restriction put a limitation on the size of the wake panels.

Computational Details

The surface panel calculations were done on an SGI 4D-320 VGX machine. The computational time for one angle of attack and one wake iteration for the high lift configuration was typically about 1.75 hours. Each case was run for 6 wake iterations.

The Euler calculations were done on a CRAY-YMP computer. The convergence history for both the explicit and implicit Euler calculations for the case of one angle of attack are presented in Fig. 14. The results presented in the figure correspond to the case of $\alpha = 7.617^{\circ}$. The implicit code required about 4 times the memory compared to the explicit version of the program. The computations were performed with a CFL number of 3.0. The solutions were started from free stream initial conditions in both the implicit and explicit calculations. The explicit calculations were stopped after the RMS average value of all the residuals (L_2-norm) decreased by about 1.7 orders of magnitude and since the calculations did not show any signs of further reduction in residuals. On the other hand the implicit calculations were run until the RMS average value of all the residuals (L_2-norm) decreased by about 5.2 orders of magnitude. Fig. 15 shows the convergence history of the lift, drag and moment coefficients for the explicit and implicit calculations. As it is seen in Fig. 15 the lift and moment coefficients have settled down after about 25000 CPU secs for the implicit calculations with residuals reduced by about 3 orders of magnitude (see Fig. 14). The explicit code took about 75000 CPU secs for the lift, drag and pitching moment coefficients to settle down, about 3 times more than the CPU time taken by the implicit version.

Summary

Two computational methods, a surface panel method and an Euler method employing unstructured grid methodology were used to analyze a subsonic transport aircraft in cruise and high-lift conditions. The computational results were compared with two separate sets of flight data obtained for the cruise and high-lift configurations. For the cruise configuration, the surface pressures obtained by the panel method and the Euler method agreed fairly well with results from flight test on the fuselage. However, for the high-lift configuration, considerable differences were observed when the computational surface pressures were compared with the results from high-lift flight test.

On the upper surface of all the elements the panel method predicted slightly higher suction compared to the Euler method. On the lower surface of all the elements with the exception of the slat, both the panel and Euler methods predict pressures which are in good agreement with flight data. On the upper surface of the slat, pressure coefficients obtained by both the Euler and panel methods do not agree with the results of the flight tests. A sensitivity study of the upward deflection of the slat from the 40° flap setting suggested that the differences in the slat deflection between the computational model and the flight configuration could be one of the sources of this discrepancy.

In the computational investigations, the panel method, VSAERO predicted higher suction on the upper surfaces than the Euler methods. Some of these differences could be attributed to the wake treatments in the panel method. It was found that the "Global" wake grid planes restricted the total number of wake panels and hence the size of the wake panels immediately aft of the trailing edges of the lifting elements. The block size in Gauss-Siedel solution put a restriction on the number of panels allowed in the streamwise direction. This limitation was found to be very critical for part-span high-lift configurations. Convergence of wakes to non-unique wake shapes have raised questions about the uniqueness and the accuracy of the solutions.

The computation time for the implicit version of the Euler code was about 1/3 the time taken by the explicit version though the implicit code required 4 times the memory taken by the explicit version.

Acknowledgments

The research was supported by NASA Langley Research Center under NASA Contract NAS1-19672 to ViGYAN, Inc., Hampton, Virginia. The author wishes to acknowledge Mr. Arild Bertelrud and Mr. Long Yip of NASA Langley Research Center for providing flight data. The author would like to thank Mr. Dan Strash of AMI, Inc., for several useful suggestions during the course of this work. The author would like thank Dr. Shahyar Pirzadeh of ViGYAN, Inc., for assistance in generating the unstructured grid and Dr. Neal Frink for providing the implicit USM3D code.

References

1. Dilner, B.; May, F.W.; and McMasters, J.H.: Aerodynamic Issues in the Design of High -Lift Systems for Transport Aircraft. AGARD CP 365, May 1984.
2. Vijgen, P.M.H.W.; Hardin, J.D.; and Yip, L.P.: Flow Prediction over a Transport Multi-Element High-Lift System and Comparison with Flight Measurements. Fifth Symposium on Numerical and Physical Aspects of Aerodynamic Flows, Long Beach, CA, 1992
3. Yip, L.P.; Vijgen, P.M.H.W.; Hardin, J.D.; and van Dam, C. P: Subsonic High-Lift Flight Research on the NASA Transport Systems Research Vehicle (TSRV). AIAA Paper 92-4103, August, 1992
4. Morgan, H.L., Jr.: A Computer Program for the Analysis of Multi-Element Airfoils in Two-Dimensional Subsonic, Viscous Flows. NASA SP 347, March 1975.
5. Brune,.W.; and McMasters, J.H.: Computational Aerodynamics Applied to High-Lift systems in Applied Computational Aerodynamics. Progress in Astronautics and Aeronautics, Vol. 125, pp. 389-433, AIAA 1990.
6. Mavriplis, D.J.; and Martinelli, L.: Multigrid Solution of Compressible Turbulent Flows on Unstructured Meshes Using a Two-Equation Model. AIAA Paper 91-0237, January, 1991.
7. Drela, M.: Newton Solution of Coupled/Inviscid Multi-Element Airfoil Flows. AIAA Paper 90-1470, June 1990.
8. Cebeci, T.; Chang, K.C.; Clark, R.W.; and Halsey,N.D.: Calculation of Flow over Multielement Airfoils at High Lift. J. Aircraft, Vol. 24, No. 8, pp. 546-551, August, 1987.
9. Rogers, S. E.; Wiltberg, N. L.; Kwak. D.: Efficient Simulation of Incompressible Viscous Flow over Multi-Element Airfoils. Fifth Symposium on Numerical and Physical Aspects of Aerodynamic Flows, California State University, Long Beach, CA, January 1992.
10. Bertelrud, A.; Watson, R.D.; and McGinley, C.B.: Flow Measurements on the Fuselage of a Boeing 737 Airplane. AIAA Paper 89-0209, January, 1989.
11. Maskew, B: Program VSAERO, A Computer Program for Calculating the Nonlinear Aerodynamic Characteristics of Arbitrary Configurations. NASA CR-166476, November, 1982.
12. Frink, N.T.; Parikh, P.; and Pirzadeh, S.: A Fast Upwind Solver for the Euler Equations on Three-Dimensional Unstructured Meshes. AIAA Paper 91-0102, January, 1991.
13. Frink, N.T.; Personal Communications.
14. Anderson, W. K.: Grid Generation and Flow Solution Method for Euler Equations on Unstructured Grids, NASA TM-4295, April, 1992.
13. Parikh, P.; Pirzadeh, S.; and Lohner, R.: A Package for 3-D Unstructured Grid Generation, Finite-Element Flow Solutions, and Flow Field Visualization. NASA CR-182090, September 1990.
14. Pirzadeh, S: Recent Progress in Unstructured Grid Generation. AIAA Paper 92-0445, January, 1992.
15. Parikh, P.; Pirzadeh, S.; and Frink, N.T.: Unstructured Grid Solutions to a Wing/Pylon/Store Configuration Using VGRID3D/USM3D. AIAA Paper 92-4572, August, 1992.

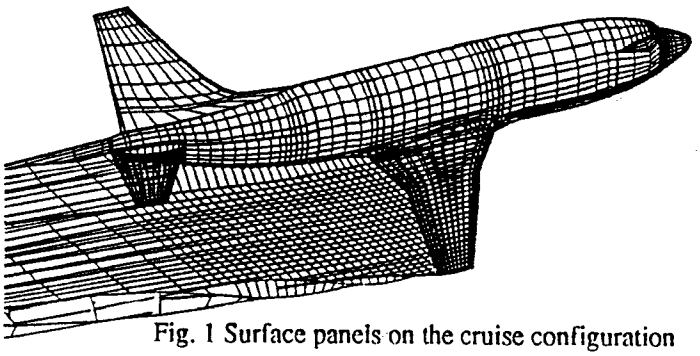

Fig. 1 Surface panels on the cruise configuration

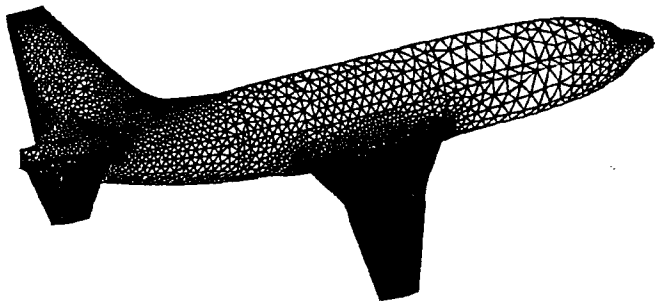

Fig. 2 Unstructured surface grid on the cruise configuration

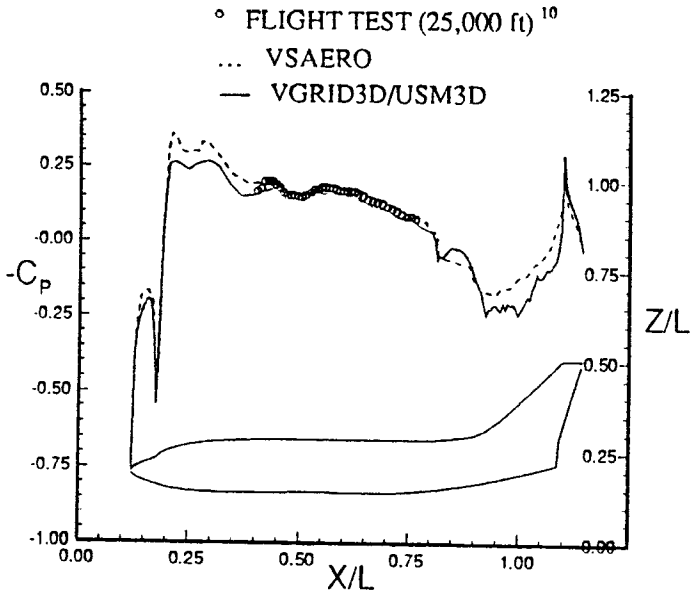

Fig. 3 Pressure distribution on the top symmetry line of the fuselage (α=6.87°, M=0.5, 2Y/b=0)

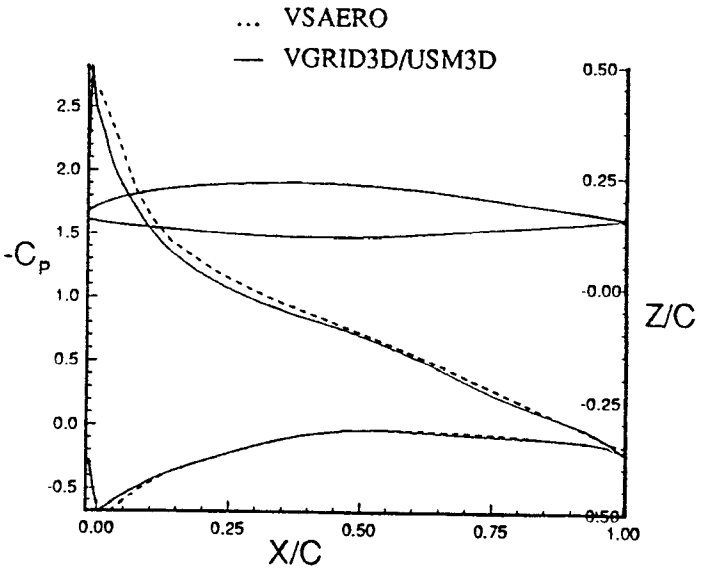

Fig.4 Pressure distributions on the wing at the spanwise section 2Y/b=0.6 (α=6.87°, M=0.5)

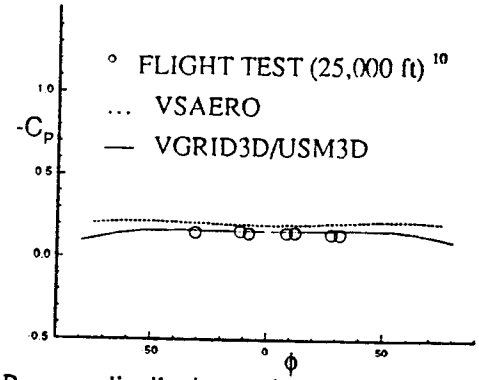

Fig.5 Pressure distribution on the fuselage at longitudinal section X/L=0.402, α=6.87°, M=0.5

Fig.6a

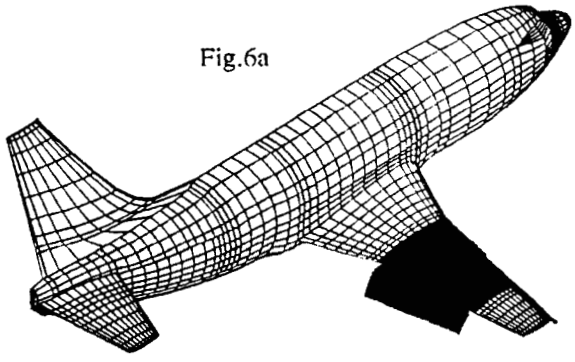

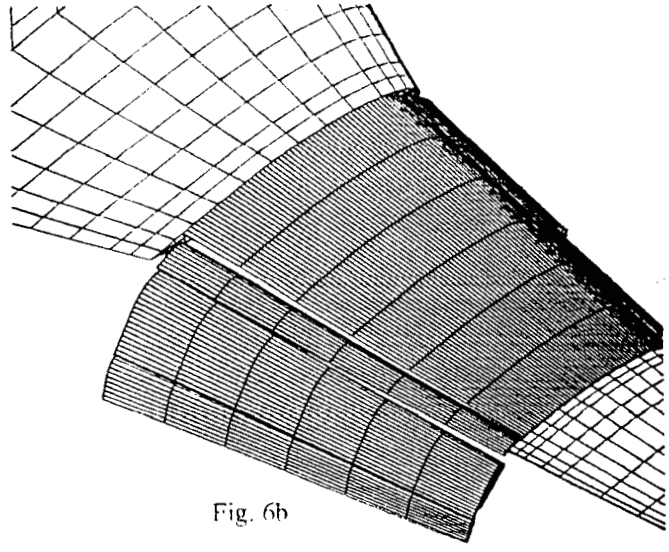

Fig. 6b

Surface panels on the high lift configuration

Fig. 7a

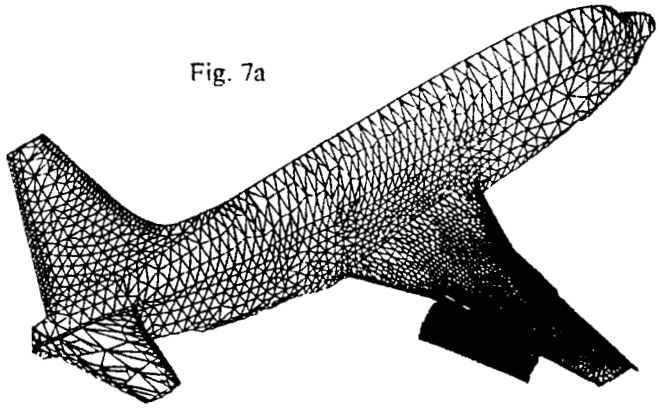

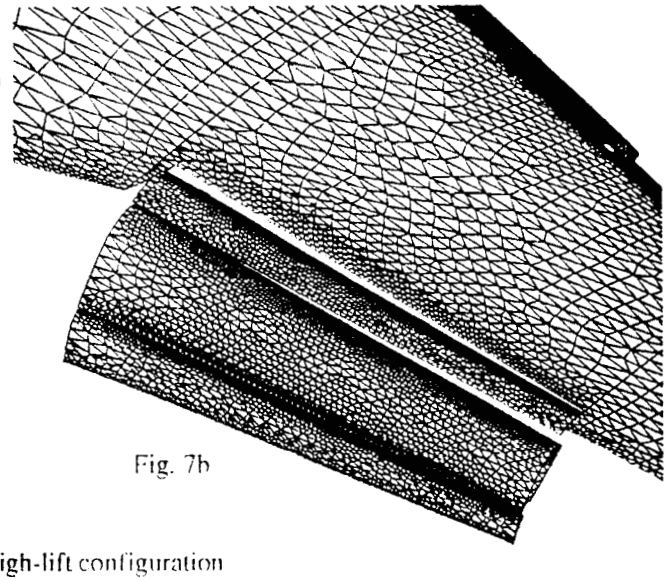

Fig. 7b

Unstructured surface grid on the high-lift configuration

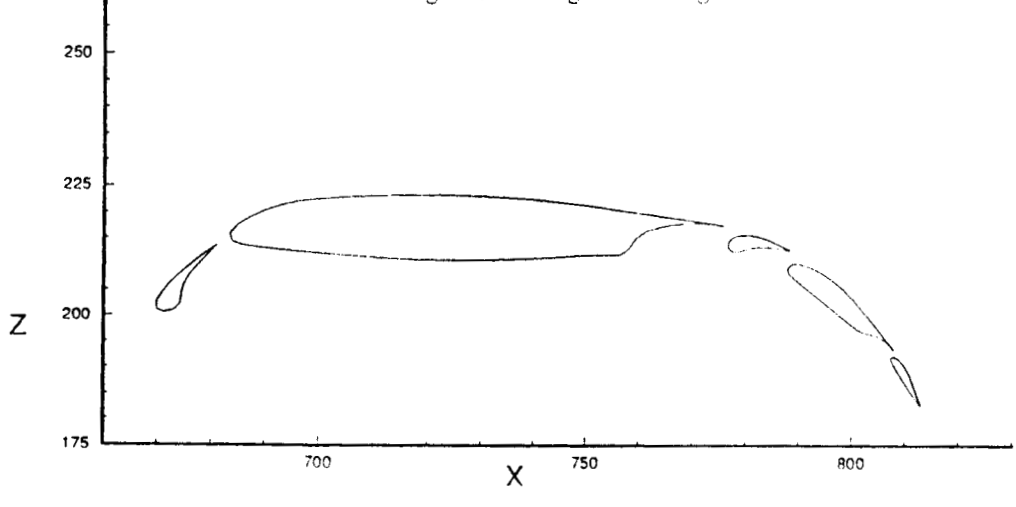

Fig. 8 Sectional view of the multi-element wing (2Y/b=0.6)

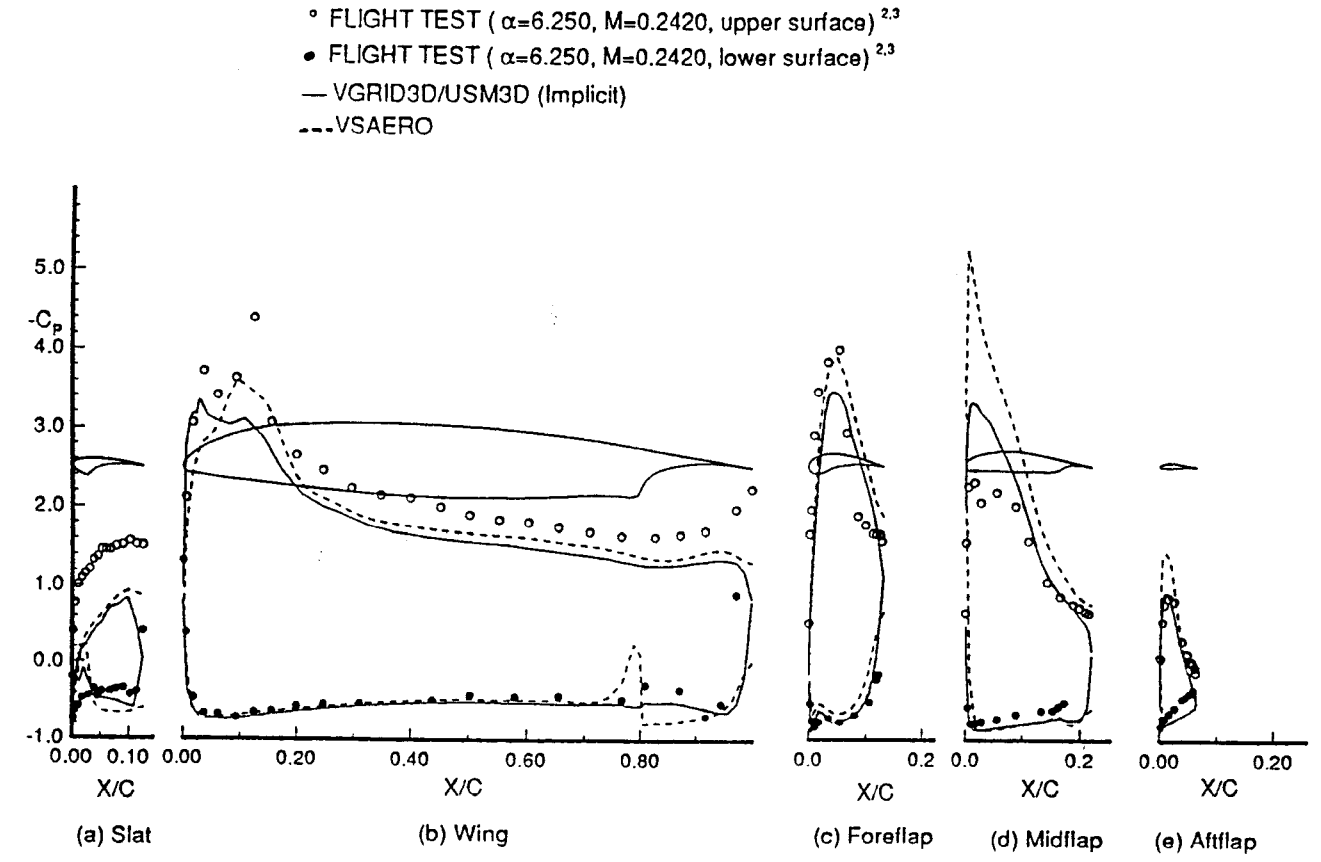

Fig. 9 Comparisons of the pressure distributions on the high-lift configuration
40° Flap setting, 2Y/b=0.6, α=6.250°

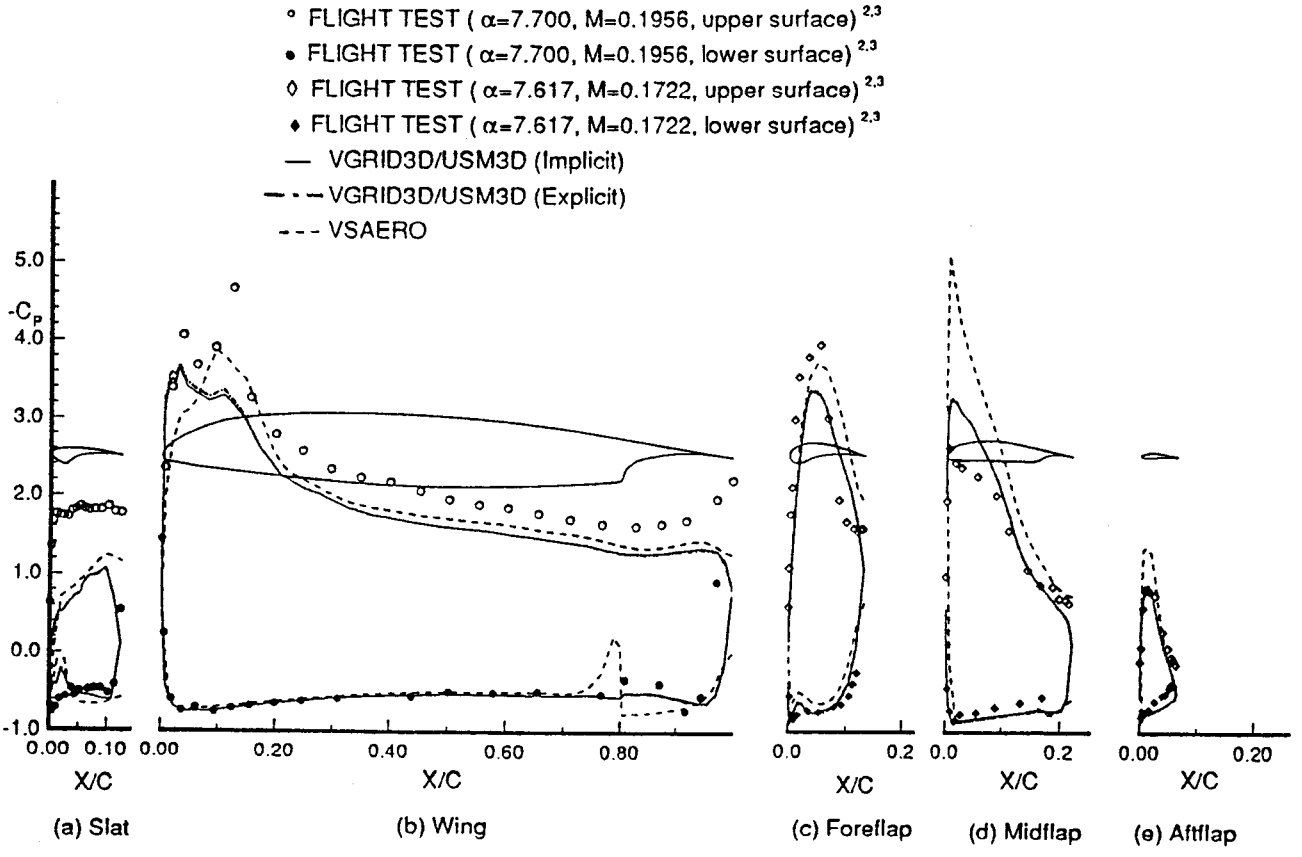

Fig. 10 Comparisons of the pressure distributions on the high-lift configuration
40° Flap setting, 2Y/b=0.6, α=7.617°

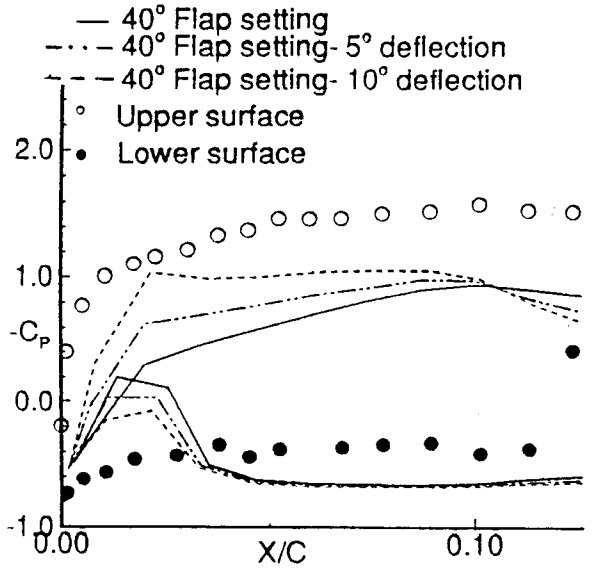

Fig. 11 Sensitivity of the slat pressures due to slat deflections
α=6.250°, M=0.2420, 40° Flap setting

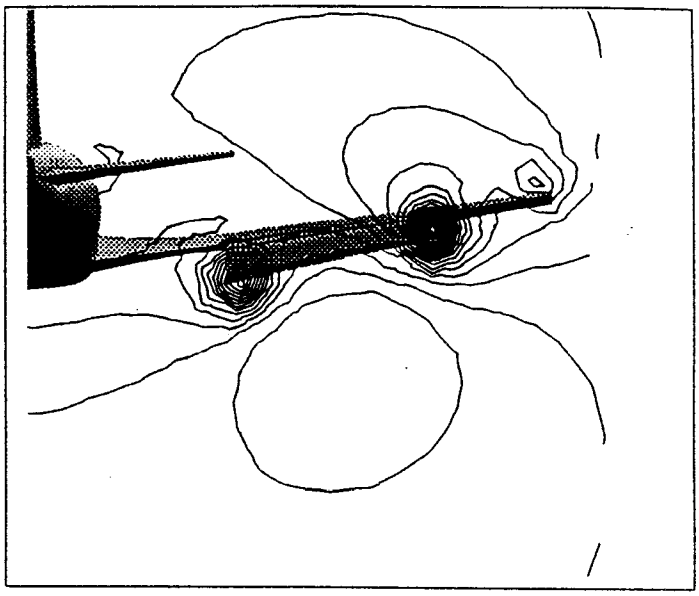

Fig. 13 Contours of total pressure at X/L=0.828 for the high-lift configuration
α=7.617°, M=0.1722, 40° Flap setting

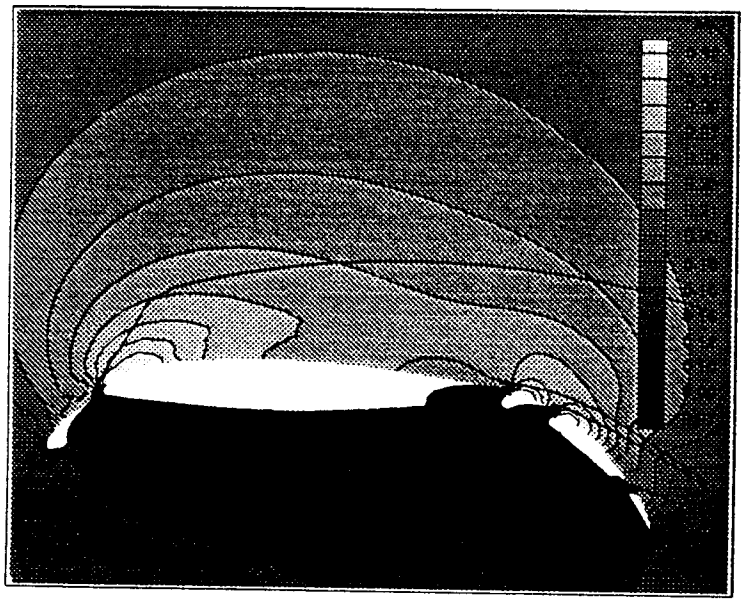

Fig.12 Contours of Mach number around the multi-element wing from Euler calculations
α=7.617°, M=0.1722, 40° Flap setting

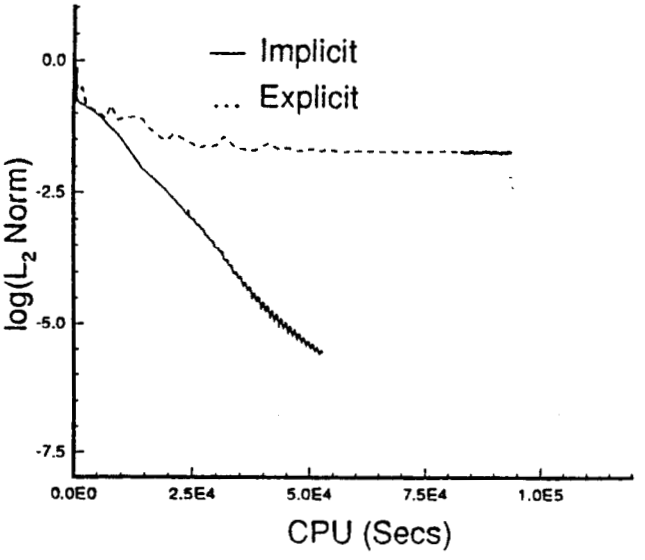

Fig. 14 Comparisons of residuals from the explicit and implicit Euler solutions
(α=7.617, M=0.1722, 40° flap setting)

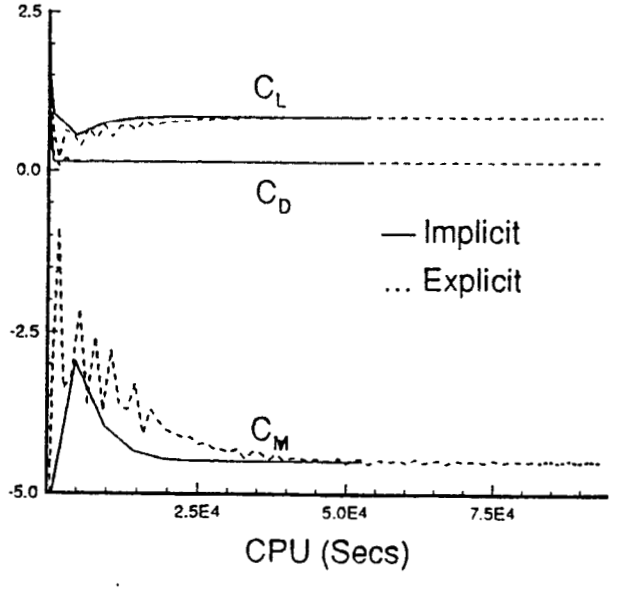

Fig. 15 Convergence history of lift, drag and moment coefficients from the implicit Euler calculations
(α=7.617, M=0.1722, 40° flap setting)